Weyl's theory applied to the Stark effect in the hydrogen atom*

Michael Hehenberger, Harold V. McIntosh,†‡ and Erkki Brändas
Quantum Chemistry Group, Uppsala University, Uppsala 1, Sweden
(Received 17 December 1973)

A short review of Hermann Weyl's theory for singular second-order differential equations is given and its numerical aspects are discussed. It is pointed out that this method is suitable for the treatment of perturbations which make the spectrum continuous. The Stark effect on the ground state of the hydrogen atom is taken as an example. The spectral density, the imaginary part of Weyl's "m function," is calculated numerically using Runge-Kutta integration and Airy integrals for the asymptotic region. Showing δ-function-like behavior with poles of m on the real axis for the discrete levels, the spectral density involves approximate Lorentzians for the metastable states of the continuous spectrum, corresponding to poles of m in the complex plane. Trajectories of these poles for electric fields up to 0.25 a.u. are shown for the one-dimensional as well as for the full three-dimensional problem.

I. INTRODUCTION

In the first sections we discuss theoretical and numerical aspects of Weyl's theory for singular self-adjoint second-order differential equations.[1] While well known to and frequently used by mathematicians since 1910, Weyl's results do not seem to have received much attention by physicists and chemists.

This theory is not only very interesting from the theoretical point of view, but also highly practical as a numerical method. A computer program, SECO, has been developed and was tested on the radial equation of the simple hydrogen atom.

One of the special features of Weyl's theory is that it requires a complex parameter and complex solutions to the differential equation, making it a natural tool for the treatment of "metastable states." By keeping a nonzero imaginary part in the "complex eigenvalue," square-integrability can still be ensured even for the continuum.

Since the hydrogen atom perturbed by an electric field is a prototype for the change of a discrete spectrum into a continuous one, we have chosen the Stark effect as an application for our numerical methods. In general terms this problem has already been analyzed by Titchmarsh. In a series of articles entitled "Theorems on Perturbation Theory," he devoted three papers[2-4] to the study of perturbations which make the spectrum continuous. The last one[4] deals with the Stark effect and concludes that the poles of the perturbed Green's function no longer are situated on the real axis as they are for the unperturbed one, but have moved away into the complex plane.

The main objective of our present treatment is to replace his estimates by accurate numbers and to trace the trajectory of the complex pole as the field strength increases. Physically, these poles contain very important information: Their real part is the resonance energy of the metastable state, associated with the least amount of leakage through the potential barrier produced by the electric field, whereas the imaginary part determines the lifetime.

II. WEYL'S LIMIT POINT–LIMIT CIRCLE THEORY

For a detailed treatment we refer to Weyl's original paper,[1] to Titchmarsh's book,[5] and to Chap. 9 of Coddington and Levinson.[6] In the following only the main results are quoted. The notation is very close to the one employed in Ref. 6.

We consider the second-order differential equation

$$L[u] = -(pu')' + qu = \lambda u, \tag{1}$$

where

$$\lambda = E + i\epsilon \quad (\epsilon \neq 0), \tag{2}$$

and $p(t)$ and $q(t)$ are real and continuous on $[0, \infty)$. In order to discuss the general solution, we start from two linearly independent solutions $\varphi(t;\lambda)$ and $\psi(t;\lambda)$, which are determined by the initial conditions

$$\begin{bmatrix} \varphi & \psi \\ p\varphi' & p\psi' \end{bmatrix}(0;\lambda) = \begin{bmatrix} \sin\alpha & \cos\alpha \\ -\cos\alpha & \sin\alpha \end{bmatrix} \tag{3}$$

$$(-\pi/2 \leq \alpha < \pi/2).$$

Any solution of (1), except ψ, can be written as

$$\chi(t;\lambda) = \varphi(t;\lambda) + m\psi(t;\lambda). \tag{4}$$

Imposing on χ the real boundary condition at $t = b$,

$$\cos\beta\,\chi(b;\lambda) + \sin\beta\, p(b)\chi'(b;\lambda) = 0 \tag{5}$$

$$(-\pi/2 \leq \beta < \pi/2),$$

we obtain

$$\mathrm{Im}[-(p\chi'/\chi)_{t=b}]=0\,, \tag{6}$$

which can also be written as

$$[\chi\chi](b)=0 \tag{7}$$

if one defines the square bracket by

$$[uv]=p(uv'^{*}-u'v^{*})\,. \tag{8}$$

The asterisk denotes complex conjugate quantities. Inserting (4) into (7), one arrives at

$$\{[\varphi\varphi]+m[\psi\varphi]+m^{*}[\varphi\psi]+mm^{*}[\psi\psi]\}_{t=b}=0\,. \tag{9}$$

After division by $[\psi\psi](b)$ and some manipulations involving the use of *Green's formula*

$$\int_0^b \{v^{*}L[u]-(L[v])^{*}u\}\,dt=[uv](b)-[uv](0) \tag{10}$$

to verify

$$[\varphi\psi^{*}](t)=1 \quad (\text{all } t)\,, \tag{11}$$

we finally obtain

$$\left(m+\frac{[\varphi\psi]}{[\psi\psi]}\right)\left(m+\frac{[\varphi\psi]}{[\psi\psi]}\right)^{*}\Bigg|_{t=b}=\frac{1}{|[\psi\psi](b)|^2}\,, \tag{12}$$

which is the equation for a *circle in the complex m-plane with center*

$$c_b=-[\varphi\psi](b)/[\psi\psi](b) \tag{13}$$

and radius

$$r_b=1/|[\psi\psi](b)|\,. \tag{14}$$

When inserting our solutions φ and ψ of (1), both associated with the same parameter λ, *Green's formula* (10) reads

$$(\lambda-\lambda^{*})\int_0^b \varphi\psi^{*}\,dt=[\varphi\psi](b)-[\varphi\psi](0)\,, \tag{15}$$

which shows the connection between inner products and boundary values. Employing this technique, it is easy to show that Weyl's circle must shrink as the interval increases, leading to the following two cases for the infinite interval.

(a) As $b\to\infty$, r_b stays finite; i.e., one has a *limit circle*. Since

$$\int_0^b |\psi|^2\,dt=\frac{[\psi\psi](b)}{\lambda-\lambda^{*}}\,, \tag{15'}$$

it is seen from (14) that $\psi\in L^2(0,\infty)$. Since, further, χ, as defined by (4) with m lying on the circle, is square-integrable, *all* solutions of (1) must be square-integrable.

(b) As $b\to\infty$, r_b tends to zero; i.e., one has a *limit point*. Equations (14) and (15′) imply that the norm of ψ will be infinite for this case. Still, $\chi=\varphi+m_\infty\psi$ (where m_∞ denotes the limit point) is square-integrable and since χ and ψ are linearly independent, χ must be the unique square-integrable solution.

According to Coddington and Levinson there is a rather simple rule for the distinction of the two cases mentioned above: If $q(t)\geq -k$, where k is a positive constant, and

$$\int^{\infty} p^{-1/2}\,dt=\infty\,,$$

then L is in the limit-point case at infinity. For the special case $p(t)=1$ for $0\leq t<\infty$ the rule simplifies to : If $q(t)\geq -kt^2$ for some positive constant k, then L is in the limit-point case at infinity.

Weyl's theory establishes a connection between classical Sturm-Liouville theory for a finite interval and the complex theory for an infinite interval. Instead of (1) write

$$L[u]=\omega u \tag{16}$$

where ω is real. Define an eigenvalue problem on $[0,b]$ by adding to (16) the boundary conditions

$$\sin\alpha\,u(0)-\cos\alpha\,p(0)u'(0)=0\,, \tag{17}$$

$$\cos\beta\,u(b)+\sin\beta\,p(b)u'(b)=0 \tag{18}$$

$$(-\pi/2\leq\alpha,\ \beta<\pi/2).$$

Then there exists a sequence

$$\{\omega_{bk}\} \quad (k=1,2,\ldots) \tag{19}$$

of eigenvalues and a complete and orthonormal set

$$\{u_{bk}\} \quad (k=1,2,\ldots) \tag{20}$$

of eigenfunctions.

Consider solutions $\psi(t;\omega_{bk})$ characterized by the same initial conditions (3) as Weyl's complex solution $\psi(t;\lambda)$. Since $\psi(t;\omega_{bk})$ satisfies the left boundary condition (17), we have

$$u_{bk}(t)=c_{bk}\psi(t;\omega_{bk}) \tag{21}$$

with a value of c_{bk} independent of t. Any continuous function $f(t)$ which vanishes outside $0\leq t\leq c$ $(0<c<b)$ can be expanded in the orthonormal set $\{u_{bk}\}$, leading to the *completeness relation (Parseval equality)*

$$\int_0^b |f(t)|^2\,dt=\sum_{k=1}^{\infty}\left|\int_0^b u_{bk}(t)f(t)\,dt\right|^2. \tag{22}$$

By means of (21), the right-hand member becomes

$$\sum_{k=1}^{\infty}|c_{bk}|^2\left|\int_0^b \psi(t;\omega_{bk})f(t)\,dt\right|^2. \tag{23}$$

Finally, defining

$$g(\omega)=\int_0^\infty \psi(t;\omega)f(t)\,dt \tag{24}$$

and $\rho_b(\omega)$, the *spectral function* as a monotonic nondecreasing step function of ω having jumps of $|c_{bk}|^2$ at each eigenvalue ω_{bk} and being constant otherwise, (22) can be rewritten as

$$\int_0^\infty |f(t)|^2\,dt=\int_{-\infty}^\infty |g(\omega)|^2\,d\rho_b(\omega)\,. \tag{25}$$

In the limit $b\to\infty$ the right-hand member must be written as a *Stieltjes integral* involving the monotonic nondecreasing function $\rho(\omega)$.

To establish the desired connection to Weyl's complex theory, we first observe that $\psi(t;\lambda)$ defined by (3) satisfies the left boundary condition (17) of the real problem. However, the function satisfying the right boundary condition (18)—which has been chosen equal to (5) for the purpose of comparison—is $\chi(t;\lambda)$ given by (4) and with a value of $m(\lambda, b, \beta)$ situated on Weyl's circle. If $E=\mathrm{Re}(\lambda)$ equals a Sturm-Liouville eigenvalue, both ψ and χ tend to the corresponding eigenfunction in the limit $\epsilon=\mathrm{Im}(\lambda)\to 0$. This leads us to the conclusion that the meromorphic function $m(\lambda, b, \beta)$ has poles whenever

$$\lambda=\lim_{\epsilon\to 0}(\omega_{bk}+i\epsilon)\quad (k=1, 2, \ldots)\,. \tag{26}$$

So the poles of $m(\lambda, b, \beta)$ are the zeros of

$$\cos\beta\,\psi(b;\lambda)+\sin\beta\,p(b)\psi'(b;\lambda)\,.$$

Again consider the Parseval equality, but now for the complex-valued function $\chi(t)$:

$$\int_0^b |\chi(t)|^2\,dt=\sum_{k=1}^\infty \left|\int_0^b u_{bk}^*(t)\chi(t)\,dt\right|^2. \tag{22'}$$

Being the eigenfunctions of the Sturm-Liouville problem (16)–(18), the u_{bk}'s are real and the asterisk can be omitted in (22'). Use of the Green's formula in both the left- and the right-hand members of (22'), together with the fact that χ and u_{bk} satisfy the same right boundary condition, leads to the important relation

$$\mathrm{Im}[m(\lambda, b, \beta)]=\int_{-\infty}^\infty \frac{\epsilon\,d\rho_b(\omega)}{|\omega-\lambda|^2}$$

$$=\int_{-\infty}^\infty \frac{\epsilon\,d\rho_b(\omega)}{(\omega-E)^2+\epsilon^2}\,. \tag{27}$$

Letting b go to infinity and assuming the *limit-point case*, we obtain

$$\mathrm{Im}[m_\infty(E+i\epsilon)]=\int_{-\infty}^\infty \frac{\epsilon\,d\rho(\omega)}{(\omega-E)^2+\epsilon^2}\,. \tag{28}$$

Finally, if E_α and E_β both denote points of continuity for the spectral function $\rho(\omega)$, we may integrate over E, take the limit $\epsilon\to 0$, and get

$$\rho(E_\beta)-\rho(E_\alpha)=\lim_{\epsilon\to 0}\frac{1}{\pi}\int_{E_\alpha}^{E_\beta}\mathrm{Im}[m_\infty(E+i\epsilon)]\,dE\,, \tag{29}$$

which is an example of the Stieltjes inversion formula. Equations (28) and (29) indicate that the imaginary part of Weyl's m function can be identified with the spectral density. It is of central importance in the theory and also the main tool in our numerical applications.

Next we consider the angle α in the initial conditions (3) in more detail. For any α and any complex λ it is possible to find a solution $\chi_\alpha=\varphi_\alpha+m_\alpha\psi_\alpha$ which satisfies a given right boundary condition. However, among all "initial phases" α in the interval $-\pi/2\le\alpha<\pi/2$, there exists, for any given $\lambda=E+i\epsilon$, a unique "quantizing phase" α_Q such that the m function associated with α_Q has a pole at E. In other words, α_Q is the angle one has to use in the left boundary condition (18) to make E a Sturm-Liouville eigenvalue. To understand this, one has to remember that the discrete spectrum of a differential operator is easily shifted just by changing the boundary conditions.

In order to derive an explicit expression for α_Q, we first have to find out how $m_\alpha=m_\alpha(\lambda, b, \beta)$ varies with the initial phase α. As indicated by Eq. (27), it should be possible to detect the poles of m by looking at its imaginary part. For $\alpha=\alpha_Q$ and $\epsilon\to 0$, it tends to be a δ function which becomes approximately a Lorentzian with increasing half-width for increasing distance ϵ from the real axis.

To proceed, we first have to express our complex solution matrix

$$\underline{Z}_\alpha(b)=\begin{bmatrix}\varphi_\alpha & \psi_\alpha\\ p\varphi'_\alpha & p\psi'_\alpha\end{bmatrix}(b) \tag{30}$$

in terms of $\underline{Z}_0(b)$ (the subscript 0 stands for α_0), where α_0 is an arbitrarily fixed angle, and the difference

$$\gamma=\alpha-\alpha_0\,. \tag{31}$$

Then

$$\underline{Z}_\alpha(b)=\underline{Z}_0(b)\underline{Z}_0^{-1}(0)\underline{Z}_\alpha(0), \tag{32}$$

where $\underline{Z}_0(0)$ and $\underline{Z}_\alpha(0)$ are initial matrices (3) characterized by the phases α_0 and α, respectively. Using the addition theorems for trigonometric functions, we get

$$\begin{bmatrix} \varphi_\alpha & \psi_\alpha \\ p\varphi'_\alpha & p\psi'_\alpha \end{bmatrix}(b) = \begin{bmatrix} \varphi_0\cos\gamma + \psi_0\sin\gamma & -\varphi_0\sin\gamma + \psi_0\cos\gamma \\ p(\varphi'_0\cos\gamma + \psi'_0\sin\gamma) & -p(\varphi'_0\sin\gamma - \psi'_0\cos\gamma) \end{bmatrix}(b). \tag{33}$$

From (4) and (5) we derive

$$m_\alpha = -\left.\frac{\cot\beta\varphi_\alpha - p\varphi'_\alpha}{\cot\beta\psi_\alpha - p\psi'_\alpha}\right|_{t=b}. \tag{34}$$

Inserting (33), we finally find

$$m_\alpha = \frac{m_0\cot\gamma - 1}{m_0 + \cot\gamma} = \frac{m_0 - \tan\gamma}{m_0\tan\gamma + 1} \tag{35}$$

for m as a function of the phase.

As γ varies from $-\pi/2$ to $\pi/2$, $\tan\gamma$ lies between $-\infty$ and $+\infty$ and (35) may hence be compared with the general linear fraction

$$w = \frac{az+b}{cz+d} \quad (-\infty < z < \infty), \tag{36}$$

which represents a mapping of the real z-axis on a circle in the complex w plane with radius

$$r = \frac{|ad - bc|}{|c^*d - cd^*|} \tag{37}$$

and center

$$C = \frac{ad^* - bc^*}{dc^* - cd^*}. \tag{38}$$

For our special case (35), the formulas (37) and (38) become

$$r = \frac{|1 + m_0^2|}{|m_0^* - m_0|}, \tag{37'}$$

$$C = \frac{1 + m_0 m_0^*}{m_0^* - m_0} = i\frac{1 + m_{01}^2 + m_{02}^2}{2m_{02}}, \tag{38'}$$

where m_{01} and m_{02} denote real and imaginary parts of m_0, respectively. Equation (38') implies that the circle generated as α varies must be centered about the imaginary axis. Consequently, the extrema of the imaginary part correspond to the zeros of the real part of m_α.

When $\alpha = \alpha'_Q$, the highest point on the circle must be obtained. Using (37') and (38'), it is further seen that there exists the simple connection

$$\max \mathrm{Im}(m_\alpha) = [\min \mathrm{Im}(m_\alpha)]^{-1} \tag{39}$$

between the extremal points of the circle.

To actually derive explicit expressions for $\alpha_Q = \alpha_{\max}$ and $\alpha_{\min}$, we separate (35) into its real and imaginary parts, put the real part equal to zero or maximize the imaginary part. The resulting quadratic equation has the form

$$\cot\gamma_{1,2} = (1/2m_{01})\{1 - M_0 \pm [1 + M_0^2 + 2(m_{01}^2 - m_{02}^2)]^{1/2}\}, \tag{40}$$

where

$$M_0 = m_{01}^2 + m_{02}^2. \tag{41}$$

Equation (40) is easily programmed to determine the quantizing phase α_Q. Since $\cot(\pi/2 - \gamma) = (\cot\gamma)^{-1}$, it follows further that $m_{\max}$ and $m_{\min}$ correspond to initial phases which differ by an angle of $\pi/2$, a fact which is associated with the definitions of φ and ψ in (3).

III. WEYL'S THEORY AS A NUMERICAL METHOD

The second-order equation (1) can be rewritten in the form

$$\begin{bmatrix} \varphi & \psi \\ p\varphi' & p\psi' \end{bmatrix}' = \begin{bmatrix} 0 & 1/p \\ q - \lambda & 0 \end{bmatrix}\begin{bmatrix} \varphi & \psi \\ p\varphi' & p\psi' \end{bmatrix} \tag{42}$$

and integrated numerically. Since both complex solutions and their derivatives are required, this form seems to be the most convenient one from a computational point of view. In our program SECO the Runge-Kutta method is implemented and two alternatives are available, namely the classical fourth-order method (e.g., Ref. 7) and a sixth-order method.[8]

As apparent from Sec. II, the key quantity to be calculated is Weyl's m function. When dealing with an infinite interval and limit-point case—as is usual in most physical examples—m_∞ may be calculated by means of Eq. (13) or, even simpler, by means of

$$m_\infty(\lambda) = -\lim_{b\to\infty}\frac{\varphi(b;\lambda)}{\psi(b;\lambda)}. \tag{43}$$

This relation is easily verified, e.g., by starting from (34) and observing that β is arbitrary in the case that the circle has shrunk to a point.

To solve a given eigenvalue problem, it is convenient to utilize the idea of the quantizing phase discussed above. Letting α_L be the angle characterizing the left and α_R the one characterizing the right boundary condition, the following steps are necessary: (i) Choose a trial $\lambda = E + i\epsilon$ ($\epsilon \neq 0$); (ii) integrate from $t = 0$ out with arbitrary initial phase α_0 and determine α_Q from the value of $m_0(\lambda, b, \alpha_R)$ according to (40); (iii) compare α_Q with α_L, and if they coincide, an eigenvalue has been found.

In this fashion one may scan the entire eigenvalue spectrum. Some interpolation scheme can be used to locate the eigenvalues more precisely. Often it may be convenient or necessary (e.g., if

the potential at one end point of the interval is singular, as is the case for Coulombic problems) to divide the interval into two parts. A left and a right integration may be performed and the quantizing phases matched. Then two m functions, m_{in} and m_{out}, have to be calculated. If, as in the case of the Coulomb potential, the potential is infinite at the origin, the integration has to be interrupted at a small distance t_1 from $t=0$ and the power-series expansion around the origin used to obtain the appropriate angle β to put into $m_{in}(\lambda, t_1, \beta)$ in order to provide a left boundary condition equivalent to the requirement that the solution has to be zero at the origin.

On Figs. 1–3 the method is illustrated by means of the radial equation of the hydrogen atom,

$$\left(-\frac{d^2}{dr^2}-\frac{2}{r}+\frac{l(l+1)}{r^2}\right)P_{nl}(r)=E_{nl}P_{nl}(r), \qquad (44)$$

in which the energy is measured in rydbergs.

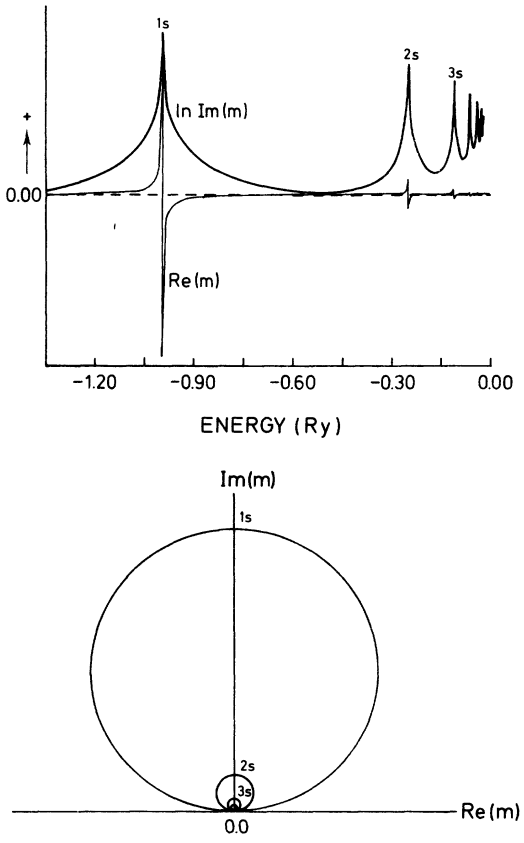

FIG. 1. (a) Real and imaginary part of Weyl's limit point for the radial equation of the unperturbed hydrogen atom. Parameters: $l=0$ (s states), $-1.35 \leq \mathrm{Re}(\lambda) < 0.0$, $\mathrm{Im}(\lambda)=10^{-3}$ Ry. Re(m) changes sign and Im(m) has maxima at the eigenvalues $E_k=-1/k^2$ Ry ($k=1, 2, \ldots$). (b) Trajectory of $m(\lambda)$ in the complex plane, same data as Fig. 1(a).

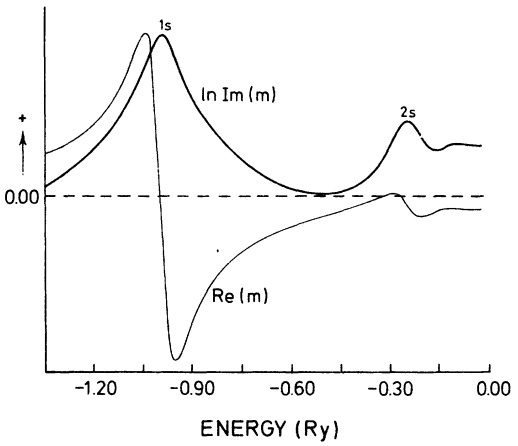

FIG. 2. Same as Fig. 1(a), except Im(λ) is 5×10^{-2} Ry. Note the bad resolution of the higher states, resulting in an asymmetric shape of Im(m).

IV. STARK EFFECT IN THE HYDROGEN ATOM: GENERAL CONSIDERATIONS

In 1913, Stark[9] observed the effect which bears his name and which comprises the changes in the spectrum of the hydrogen atom under the influence of a homogeneous electric field.

For 60 years the Stark effect has been a favorite example for application of new theories and methods. There are two main reasons responsible for this fact: The first is that the nonrelativistic problem is exactly separable (the relativistic problem is not[10]) in parabolic coordinates, and secondly,

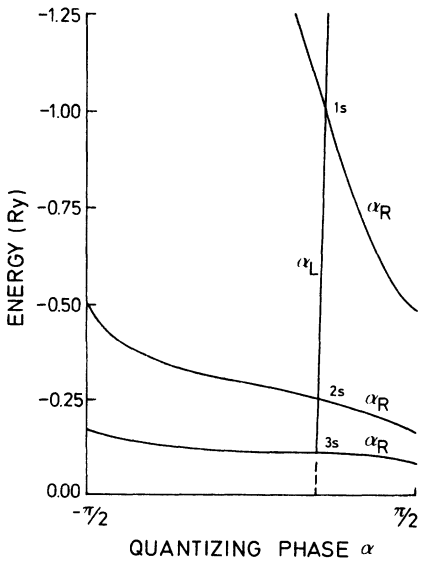

FIG. 3. Radial equation of hydrogen atom, s states. Right (α_R) and left (α_L) quantizing phases at a matching distance 0.5 a.u. from origin.

one deals with the interesting problem of a perturbation which makes the spectrum continuous. The separability had already been used by Epstein[11] and Schwarzschild[12] who in 1916 applied the "old quantum theory" of Bohr and Sommerfeld and were able to explain surprisingly well the experimental results available at that time. In 1926, Schrödinger himself[13] and further Epstein[14] and Waller[15] treated the problem by expansion-type perturbation theory, hereby neglecting complications due to the continuum.

First in 1930, when experiments with extremely high electric fields[16] could be carried out, it became obvious that conventional perturbation theory was not fully applicable. It was Lanczos[17] who clearly pointed out its limitations and who first discussed the very particular nature of the continuous spectrum of the perturbed hydrogen atom. In a series of papers he started to treat the problem by means of various approximations, involving Bessel functions of order $\frac{1}{3}$ for the asymptotic solutions and elliptic integrals for the eigenvalues. Finally, in the last paper of the series, he used the WKB technique. It is interesting to study this paper, since he even points out the similarities between the Stark effect and the problem of radioactivity as discussed by Gamow[18] and by Gurney and Condon.[19] He also gave a short treatment of the Auger effect. Many workers, especially in the last two decades, have continued along Lanczos's lines, employing the WKB approximation. Rice and Good[20] used an "improved WKB method,"[21] Alexander[22] combined the WKB solution for the asymptotic region with a highly accurate numerical method due to Rosenthal and Wilson,[23] and Hirschfelder and Curtiss[24] did essentially the same but generalized to other states than the ground state and used numerical integration of the differential equation to be solved. Berkenstein and Krieger[25] compared the WKB method with fourth-order perturbation theory. Redei[26] gave an interesting discussion of boundary conditions which could be imposed in order to ensure convergence for formal perturbation theory and Mendelsohn[27] seems to be the one who has exploited the possibilities of finite-order perturbation theory to the fullest, using "large-Z expansion theory" up to tenth order. However, at a field of 0.065 a.u. ($\sim 3.34\times 10^8$ V/cm) he was forced to the statement that "the tenth-order term gave a larger correction than the eighth-order one."

As already mentioned in the Introduction, we are essentially following Titchmarsh's analysis of the problem which is based on Weyl's theory. Before proceeding, we give a short review of the separation of the Schrödinger equation for the perturbed one-electron problem into parabolic coordinates.

For a homogeneous electric field of absolute strength F (in atomic units) in the z direction, we get, using the rydberg as the unit for energy, the Schrödinger equation

$$(\Delta + 2Z/r - 2Fz + E)\psi(\vec{r}) = 0. \tag{45}$$

There are two sets of parabolic coordinates in which (45) can be separated:

(i) *Conventional parabolic coordinates* (ξ, η, φ):

$$\begin{aligned} x &= (\xi\eta)^{1/2}\cos\varphi\,, \\ y &= (\xi\eta)^{1/2}\sin\varphi\,, \\ z &= \tfrac{1}{2}(\xi - \eta)\,. \end{aligned} \tag{46}$$

After separation of the φ-dependent part, we get, putting

$$\psi(\vec{r}) = u(\xi)v(\eta)e^{im\varphi}, \tag{47}$$

the second-order differential equations

$$\left[\frac{d}{d\xi}\left(\xi\frac{d}{d\xi}\right) + \frac{E}{4}\xi - \frac{m^2}{4\xi} - \frac{F}{4}\xi^2 + Z_1\right]u(\xi) = 0, \tag{48a}$$

$$\left[\frac{d}{d\eta}\left(\eta\frac{d}{d\eta}\right) + \frac{E}{4}\eta - \frac{m^2}{4\eta^2} + \frac{F}{4}\eta^2 + Z_2\right]v(\eta) = 0, \tag{48b}$$

which are coupled by the requirement

$$Z_1 + Z_2 = Z\,. \tag{49}$$

Substituting

$$u(\xi) = \xi^{-1/2}u_1(\xi), \tag{50a}$$

$$v(\eta) = \eta^{-1/2}v_1(\eta), \tag{50b}$$

we arrive instead at eigenvalue problems for the energy:

$$\left(\frac{d^2}{d\xi^2} + \frac{1-m^2}{4\xi^2} + \frac{Z_1}{\xi} - \frac{F}{4}\xi + \frac{E}{4}\right)u_1(\xi) = 0, \tag{51a}$$

$$\left(\frac{d^2}{d\eta^2} + \frac{1-m^2}{4\eta^2} + \frac{Z_2}{\eta} + \frac{F}{4}\eta + \frac{E}{4}\right)v_1(\eta) = 0\,. \tag{51b}$$

Even here (49) is the only condition which couples the equations. We have called the coordinates (ξ, η, φ) "conventional" ones since they have been used in all quantum-mechanical treatments of the Stark effect known to the authors. Equations (51) are very convenient because of the appearance of the energy as an eigenvalue parameter, letting them resemble the ordinary type of Schrödinger equation. For further details we refer to Bethe and Salpeter.[28]

(ii) *"Squared"*[29] *parabolic coordinates* (μ, ν, φ):

$$\begin{aligned} x &= \mu\nu\cos\varphi\,, \\ y &= \mu\nu\sin\varphi\,, \\ z &= \tfrac{1}{2}(\mu^2 - \nu^2)\,. \end{aligned} \tag{52}$$

After separation of the φ-dependent part,

$$\psi(\vec{r}) = M(\mu)N(\nu)e^{im\varphi}, \tag{53}$$

and substitutions

$$M(\mu) = \mu^{-1/2}M_1(\mu), \tag{54a}$$

$$N(\nu) = \nu^{-1/2}N_1(\nu), \tag{54b}$$

we get

$$\left(\frac{d^2}{d\mu^2} + \frac{1-m^2}{4\mu^2} + E\mu^2 - F\mu^4 + Z_1\right)M_1(\mu) = 0, \tag{55a}$$

$$\left(\frac{d^2}{d\nu^2} + \frac{1-m^2}{4\nu^2} + E\nu^2 + F\nu^4 + Z_2\right)N_1(\nu) = 0, \tag{55b}$$

where

$$Z_1 + Z_2 = 4Z. \tag{56}$$

Unfortunately, no transformation brings (55) to a form as convenient as (51). While used frequently in classical mechanics and in the "old quantum theory" (cf. Ref. 11), they seem to be less useful in quantum-mechanical treatments. Their most interesting feature is their resemblance to the radial equation of the harmonic oscillator in polar coordinates, which is important for understanding the symmetry and degeneracy of the hydrogen atom. Most of this regularity is lost in the Stark effect.

Both separation schemes were tested numerically in the present treatment. For given accuracy of the eigenvalue to be determined (known exactly in the unperturbed case), we found the "squared" coordinates to be less time consuming than the "conventional" ones. The explanation lies presumably in the faster convergence of Weyl's circle to a point due to the more rapidly increasing potential occurring in (55a) as compared with (48a).

As described below, however, for the solution of the unbounded problems, analytic representations of the asymptotic solutions were needed. The fact that it seemed to be easier to find such solutions for Eq. (51b) than for Eq. (55b), together with the advantage of using the transformed equation (51b), caused us to decide in favor of (ξ, η, φ).

V. NUMERICAL TREATMENT OF THE STARK EFFECT BY MEANS OF WEYL'S THEORY

The problem in the determination of the Stark shifts as functions of the field strength F is the necessity of simultaneously solving two equations coupled by (49), where one of the equations contains a potential which is unbounded from below. It is most convenient to use Eqs. (48a) and (51b) together. Choosing a trial input energy E_{in} for a given fixed field, (48a) can be used to determine the corresponding "effective charge" Z_1. From (49) we readily obtain $Z_2 = Z - Z_1$ and both F and Z_2 can then be used in the potential [cf. Eq. (1)]

$$q(\eta) = \frac{m^2-1}{4\eta^2} - \frac{Z_2}{\eta} - \frac{F}{4}\eta \tag{57}$$

of Eq. (51b) to determine the corresponding output resonance energy E_{out}. Only if E_{in} and E_{out} coincide, one has picked the proper value corresponding to the perturbed level $E(F)$. Only for zero field are bound states possible, whereas a nonzero field produces a continuous spectrum from $-\infty$ to $+\infty$. Physically, the continuum arises from the possibility of tunneling through a potential barrier, leading to metastable states with finite lifetimes.

From the point of view of Weyl's theory, the m function has poles on the real axis for Eq. (48a), necessitating a small imaginary part in the parameter Z_1 in order to avoid infinities when passing an actual eigenvalue. For Eq. (51b), however, the poles gradually move away from the real axis as F increases and even for $\lambda = \lim_{\epsilon \to 0}(E + i\epsilon)$ the spectral density stays finite, having Lorentzian character with a half-width increasing with the field strength.

Figures 4–6 show the function $m(E)$ corresponding to the one-dimensional problem (51b) for three different values of the electric field strength F, but with a common fixed value of the separation constant Z_2. The asymmetry of $\mathrm{Im}[m(E)]$ must be attributed to the influence of the next-higher levels and it is more pronounced for stronger fields, i.e., for larger imaginary parts of the complex pole. This effect is accompanied by an increasing distance between the zero of $\mathrm{Re}[m(E)]$ and the maximum of the spectral density $\mathrm{Im}[m(E)]$.

Figure 2 shows a similar shape of $m(E)$. However, in this case we deal with a discrete spectrum and the effects described above are introduced by

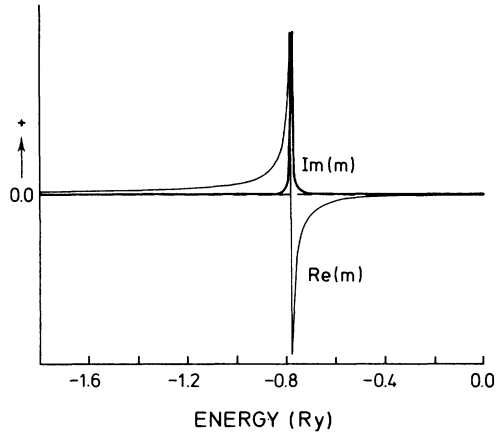

FIG. 4. Weyl's m function for the unbounded equation (51b), calculated by means of (60). Parameters: $m = 0$, $Z_2 = 0.4$, $-1.8 \leq \mathrm{Re}(\lambda) < 0.0$, $\mathrm{Im}(\lambda) = 10^{-14}$ Ry, field $F = 0.05$ a.u. Note sharp Im(m) and good coincidence of max [Im(m)] with zero of Re(m) (thinner line).

using a big value of ϵ rather than by the physical problem itself. The imaginary part ϵ used to produce Figs. 4–6 had a value of 10^{-14}. Since a change from 10^{-12} to 10^{-14} did not affect the results, we have practically extrapolated to zero.

This leads us to the interesting question whether it is possible, for continuous spectra, to proceed with $\epsilon = 0$. In case that $\lim_{\epsilon \to 0} m(E + i\epsilon)$ exists the answer is yes, but we have to realize that in establishing the limit we abandon Weyl's circle theory which rests on the requirement of a nonreal parameter λ. Numerically, a real treatment has the great advantage of being much less time consuming. With our real version of the Runge-Kutta integration program we have been able to cut down the computer time necessary to evaluate $m(E)$ almost by a factor of 2. In using real functions φ and ψ we are, however, no longer able to use formulas of type (13) or (43) for the evaluation of the m function. Instead we have utilized and extended an idea due to Titchmarsh,[2] namely, to use the known asymptotic behavior of χ to determine the desired value of m_∞.

The "generalized Titchmarsh formula" for m_∞ is obtained by considering

$$\chi = \varphi + m_\infty \psi , \tag{58}$$

$$\chi' = \varphi' + m_\infty \psi' , \tag{59}$$

and solving for m_∞, which yields

$$m_\infty = \frac{\chi\varphi' - \chi'\varphi}{\psi\chi' - \psi'\chi} . \tag{60}$$

The limit point is hence expressed as a ratio of Wronskians. The applicability of (60) rests on the knowledge of the square-integrable solution χ. Having this property, χ must vanish asymptotically, and for simple potentials leading to known analytic solutions, it is usually easy to find the desired χ_{as}. The potential (57) fortunately falls into this category. As seen from Fig. 7, it is approximately linear in the variable $\eta = r - z$ in the asymptotic region, allowing us to deal with the problem

$$\left[\frac{d^2}{d\eta^2} + \left(\lambda + d_b + \frac{F}{4}\eta\right)\right] v_1(\eta) = 0 \tag{61}$$

instead of (51b) for the interval $[b, \infty)$.

As seen from (57),

$$d_b = \frac{m^2 - 1}{4b^2} - \frac{Z_2}{b} , \tag{62}$$

a quantity which becomes more and more negligible for increasing distances b. By suitable substitutions, Eq. (61) can be transformed to Bessel's equation of order $\frac{1}{3}$ or, equivalently, to Airy's differential equation.

The first alternative has been carried out in great detail by Titchmarsh[2] and his derivation needs no repetition here. He obtains

$$v_1(\eta) \sim X^{1/3} H^{(1)}_{1/3}(X) \tag{63}$$

and

$$v_1'(\eta) \sim X^{1/3} H^{(1)}_{-2/3}(X)(\lambda + d_b + \tfrac{1}{4}F\eta)^{1/2} , \tag{64}$$

where

$$X = (8/3F)(\lambda + d_b + \tfrac{1}{4}F\eta)^{3/2} . \tag{65}$$

Jeffreys has remarked[30] that "Bessel functions of order $\frac{1}{3}$ seem to have no application except to provide an inconvenient way of expressing the Airy integrals."

Indeed, Airy functions seem to be a more natural representation of the asymptotic solutions required for our problem. We start again with (61), but introduce the substitution

$$t = (\tfrac{1}{4}F)^{-2/3}(\lambda + d_b + \tfrac{1}{4}F\eta) \tag{66}$$

$$= (\tfrac{3}{2}X)^{2/3} , \tag{67}$$

which leads to Airy's differential equation (see,

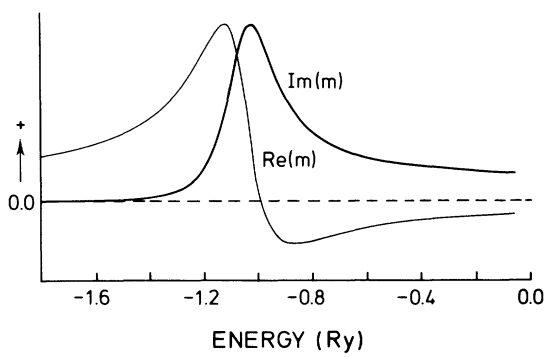

FIG. 5. Same as Fig. 4, but field increased to 0.15 a.u.

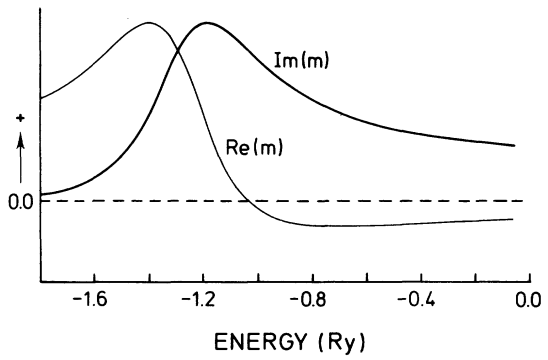

FIG. 6. Same as Figs. 4 and 5, but F changed to 0.25 a.u., the highest field considered in this paper. Very pronounced asymmetry of Im(m).

e.g., Ref. 31)

$$v_1'' + t v_1 = 0, \tag{68}$$

having the standard solutions

$$\mathrm{Ai}(-t), \quad \mathrm{Bi}(-t). \tag{69}$$

For $\arg(-t) = \pi$, both $\mathrm{Ai}(-t)$ and $\mathrm{Bi}(-t)$ are of trigonometric type. For the exponentially vanishing solution for $\eta \to \infty$, we expect therefore a linear combination of the type

$$\mathrm{Ai}(-t) - i\,\mathrm{Bi}(-t). \tag{70}$$

Using standard relations between $I_{\pm 1/3}(X)$ and the Airy integrals[31] on one hand and between $I_{\pm 1/3}(X)$ and $H_{1/3}(X)$ on the other (e.g., Ref. 32), we find the explicit connection

$$X^{1/3} H^{(1)}_{1/3}(X) = (\tfrac{2}{3})^{1/3} \sqrt{3}\, e^{-i\pi/6} [\mathrm{Ai}(-t) - i\ \mathrm{Bi}(-t)]. \tag{71}$$

The asymptotic solution to (51b) and its derivative in terms of Airy functions are hence given by

$$v_1(\eta) \sim \mathrm{Ai}(-t) - i\ \mathrm{Bi}(-t), \tag{72}$$

$$v_1'(\eta) \sim [-(\tfrac{1}{4}F)^{1/3}] [\mathrm{Ai}'(-t) - i\ \mathrm{Bi}'(-t)]. \tag{73}$$

Finally a few words about the actual computations. Since the potential (57) is singular at the origin, it is convenient to start the numerical integration at a small distance, using the power series

$$v_1(\eta) = \eta^{(m+1)/2} e^{-(-E/4)^{1/2}} \sum_{\nu=0}^{\infty} a_\nu \eta^\nu \tag{74}$$

and its derivative to determine the angle α of Eq. (3). In doing so we obtain a unimodular solution matrix corresponding to $\psi = 0$ at the origin. Then the Runge-Kutta integration of our 2×2 matrix is carried on beyond the outer classical turning point. (For very high fields above 0.15 a.u. where there are no longer any turning points, we integrated at least until the maximum of the potential barrier.) Now (60) with values of χ and χ' obtained via (72) and (73) can be used for the first time to compute m_∞. The numerical integration is then continued until m_∞ attains a stable value. The independent solutions φ and ψ (see Fig. 8) as well as χ_{as} given by (72) are oscillating functions of η, but inserted into (60) they give rise to an m function with surprisingly small fluctuations as η increases. For low fields this stability comprises 5–6 figures in its imaginary part, for high fields even more. The real part is slightly less stable. In this connection we have to mention that we used double precision arithmetic throughout on the IBM 370/155 of Uppsala Computing Center (UDAC). For the sake of comparison, both complex (with $\epsilon = 10^{-14}$) and real numerical integrations were carried out, together with numerical evaluations of real and complex Airy functions, respectively. For the calculation of real Airy functions we used Gordon's algorithm[33]; to obtain the complex ones we used a program kindly provided by UDAC. The final results for $m(E)$ turned out to coincide with at least 6–7 figures in all cases considered.

Before proceeding to the final problem of the location of the complex pole for given $m(E)$, some remarks should be made about the accuracy of our numerically obtained m function. From comparison with analytically given solutions, we know that our sixth-order Runge-Kutta method is extremely accurate, provided the step size is taken small enough in the oscillating region. A convenient test is the deviation of the Wronskian of the solution matrix from its exact value $W(\varphi, \psi) = 1$. The error intro-

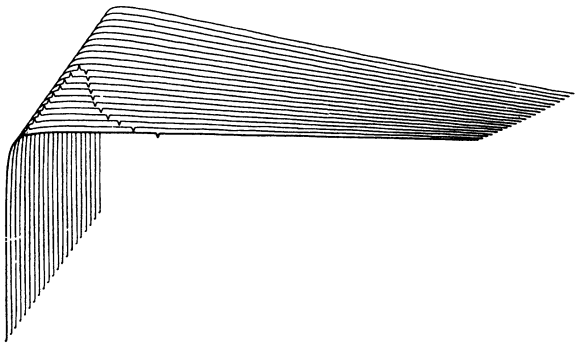

FIG. 7. $(\eta^2 - 1)/4\eta^2 - Z_2/\eta - \frac{1}{4}F\eta - \frac{1}{4}E$ displayed as a function of η, $0.0 \le \eta \le 56.0$ a.u., and for 21 values of F, $0.05 \le F \le 0.25$ a.u., where the curve $F = 0.05$ is the one closest to the observer. The zeros of this function, the classical turning points, are marked by spikes. Note their disappearance for $F > 0.15$ a.u. The values of E and Z_2 are $E = E_{\mathrm{res}}(F)$ and $Z_2 = Z_{2,\mathrm{s.c.}}(F)$.

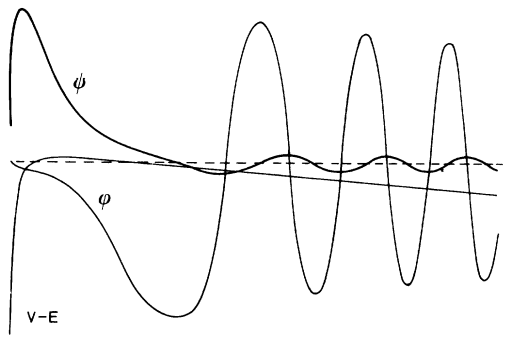

FIG. 8. Independent solutions $\psi(\eta)$ (thickest curve), $\varphi(\eta)$, and potential barrier (thinnest curve) according to Eq. (51b). Parameters: $m = 0$, $F = 0.06$ a.u., $E = E_{\mathrm{res}} = -1.018402$ Ry, $\mathrm{Im}(\lambda) = 0.0$, $Z_2 = Z_{2,\mathrm{s.c.}}$. Note inflection points for both ψ and φ at the classical turning points.

duced by the numerical evaluation of the Airy integrals is also very small. For the complex algorithm the accuracy as compared to the tables given by Miller[31] was 6–8 figures and Gordon's program is known to yield Airy integrals even with considerably greater accuracy.

The disturbing effect of the linear approximation for the potential in the asymptotic region is also very small, as could be judged from the repeated calculations of $m(E)$ with increasing distance η. Even a much more drastic approximation, namely, to put the potential outside the considered value of η equal to a constant, did not affect the results considerably. In this case the asymptotically vanishing solution χ is given by a linear combination of trigonometric instead of Airy functions.

Finally we have to turn to the problem of the actual determination of the complex poles. The asymmetry in the spectral density already mentioned above and displayed in Figs. 4–6 requires quite elaborate methods of analytical continuation. We developed a numerical procedure based on a fitting of $\mathrm{Im}[m(E)]$ to a rational fraction,

$$\mathrm{Im}[m(E)] = P_M(E)/Q_N(E), \tag{75}$$

where M and N are orders of numerator and denominator polynomials, respectively. Taking $M=0$, $N=2$, the right-hand side of (75) reduces to a Lorentzian,

$$\frac{P_0(E)}{Q_2(E)} \to \frac{a_0}{(E-E_{\mathrm{res}})^2+(\Gamma/2)^2}\,. \tag{76}$$

For small values of the electric field strength this representation is quite adequate, but as F increases M must be greater than zero to account for the asymmetric shape. Practice showed that a convenient choice is $N=2$, $M=2$, corresponding to a fitting of the rational fraction to five calculated points of $\mathrm{Im}[m(E)]$.

To obtain the desired pole $E_{\mathrm{res}}-i\Gamma/2$, we have to find the roots of the denominator polynomial $Q_N(E)$. The trajectories of these poles for the one-dimensional problem (51b) for five different constant values of the effective charge are shown in Fig. 9. As long as they stay close to the real axis, conventional expansion-type perturbation theory is capable of giving a good approximation to E_{res}, but as the poles move off, it is bound to diverge.

Figure 10 shows the trajectory of the poles for the ground state of the full three-dimensional problem (45), i.e., taking for any field F and energy E a "self-consistent" value of Z_2 which via (49) also satisfies Eq. (48a).

Figures 11 and 12 illustrate the way the resonances and half-widths can be obtained by simultaneous use of both Eqs. (48a) and (51b), the dotted lines indicating the one-dimensional half-widths. Returning to Fig. 10, we note that the curve starts at zero field at the ground-state energy −1.0 Ry, stays first close to the real axis indicating long

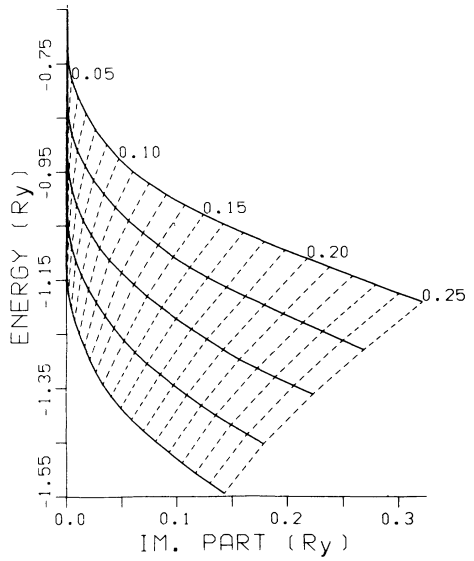

FIG. 9. Trajectories of complex poles for Eq. (51b) for five different fixed values of the separation constant Z_2. From above: $Z_2=0.4$, 0.425, 0.45, 0.475, 0.5. All five curves start from the real axis $F=0$; increases of 0.01 a.u. in F are marked and corresponding points connected by dashed lines. The numbers written at the highest curve $Z_2=0.4$ indicate F in a.u.

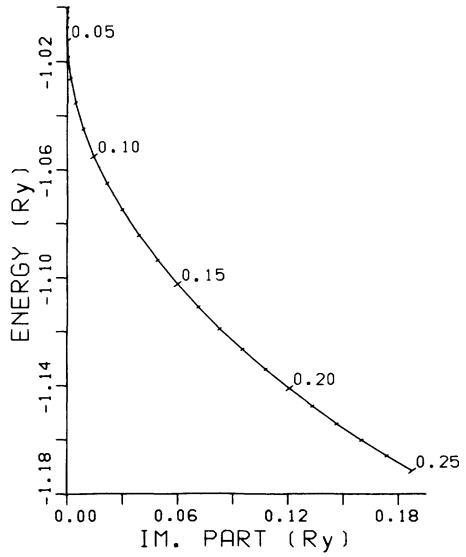

FIG. 10. Trajectory of the complex pole for the full three-dimensional problem (45); i.e., the values of Z_2 are chosen self-consistently to satisfy both Eqs. (48a) and (51b). Increases of 0.01 a.u. in F are marked; the values 0.05, 0.10, ... characterize field strengths in a.u.

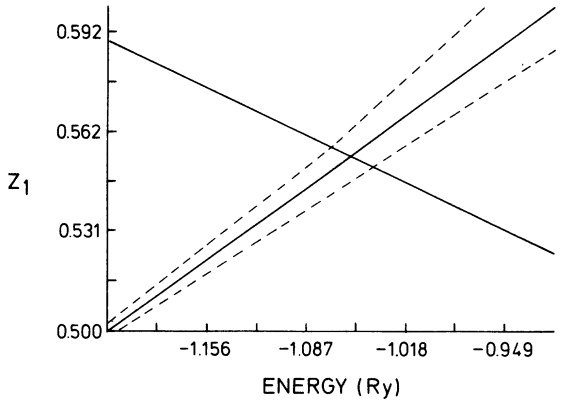

FIG. 11. Determination of resonance energy and self-consistent separation constant for $F=0.10$ a.u. The single full line represents $Z_1(E)$ as calculated from eigenvalue equation (48a); the line running from the left lower corner upwards shows $Z_1(E)=1-Z_2(E)$ as calculated from (51b). Half-widths are indicated by the dotted lines above and below.

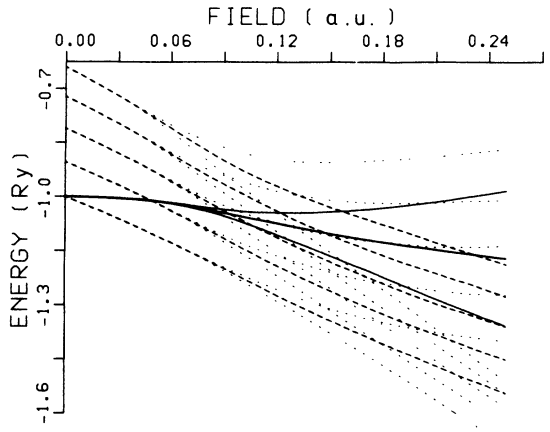

FIG. 13. "Three-dimensional" [Eq. (45); lines fully drawn] and "one-dimensional" [Eq. (51b) with fixed Z_2 $=0.4$, 0.425, 0.45, 0.475, 0.5 from above; dashed lines] energy changes due to the electric field. The thinner curves above and below indicate half-widths.

lifetimes of the metastable states, but moves for higher fields rather quickly into the complex plane. A comparison with Fig. 9 shows that the "Stark shifts" of the three-dimensional problem are much smaller than the ones for the one-dimensional one. Figure 13 makes this statement even more explicit. Apparently, the self-consistency requirement for the effective charge diminishes the effect of the electric field on the levels. Table I contains our numerical results as compared to the ones obtained by Alexander.[22] He states that he could not detect any resonance behavior above 0.12 a.u. for the field strength. As shown in Fig. 6, the resonance is still pronounced even for a field of 0.25 a.u., which was a quite arbitrary point for us to stop the calculations.

As a final illustration of our results we show the behavior of the resonance wave functions. Figure 14 gives a perspective view, where each curve corresponds to a certain field and the calculated values for E_{res} and Z_1 contained in Table I. Figure 15 is a contour plot using the same data. It is seen that outside the barrier the number of oscillations and their amplitudes increase with the field, whereas their behavior inside the potential barrier does show few changes when going from small to big perturbations.

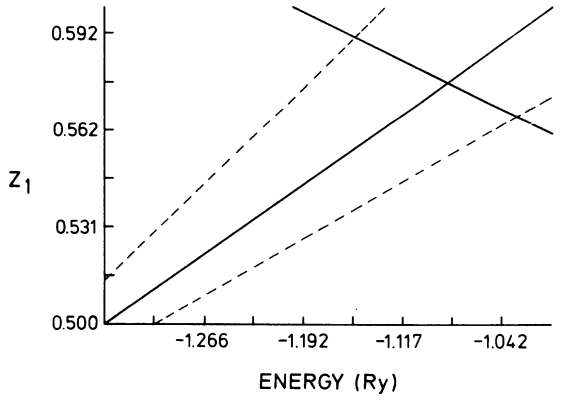

FIG. 12. Same as Fig. 11, but $F=0.15$ a.u.

TABLE I. Complex poles and separation constants for the ground state of the hydrogen atom under strong electric fields.

Field (a.u.)	Present results E_{res} (Ry)	Present results $\Gamma/2$ (Ry)	Alexander's results E_{res} (Ry)	Alexander's results $\Gamma/2$ (Ry)
0.03	−1.004 148 5	0.000 000 02	−1.004 148 546	0.000 000 02
0.04	−1.007 543 6	0.000 003 9	−1.007 543 0	0.000 004
0.05	−1.012 210 8	0.000 077 2	−1.012 21	0.000 078
0.06	−1.018 407	0.000 515	−1.018 40	0.000 52
0.07	−1.026 15	0.001 85	−1.0260	0.0019
0.08	−1.035 12	0.004 54	−1.0350	0.0046
0.09	−1.0448	0.0088	−1.0444	0.0088
0.10	−1.0549	0.0145	−1.054	0.015
0.11	−1.0649	0.0216	−1.062	0.022
0.12	−1.0748	0.0299	−1.072	0.031
0.13	−1.0843	0.0392		
0.14	−1.0935	0.0493		
0.15	−1.1024	0.0600		
0.16	−1.1108	0.0714		
0.17	−1.1189	0.0832		
0.18	−1.1266	0.0955		
0.19	−1.1340	0.1080		
0.20	−1.1411	0.1209		
0.21	−1.148	0.134		
0.22	−1.154	0.147		
0.23	−1.160	0.160		
0.24	−1.166	0.174		
0.25	−1.172	0.188		

VI. DISCUSSION

The hydrogen atom perturbed by an electric field is a classical example of the change of a discrete spectrum into a continuous one. For this reason it is suitable as an application of Weyl's theory which allows the treatment of both kinds of spectra in the same manner. The Weyl-Titchmarsh m function, whose imaginary part can be related to the spectral density, is the essential quantity in the theory. Its calculation requires a complex eigenvalue parameter λ. For the discrete spectrum, m has simple poles on the real λ axis, whereas for the continuum it may exist even on the real axis as a limiting value for $\epsilon = \mathrm{Im}(\lambda) \to 0$. By analytical continuation across the real axis it is then possible to find poles on the other half of the complex plane. The positions of these poles have physical significance in terms of resonance levels and associated lifetimes.

Although the extremely high fields considered in this paper may not have immediate interest with respect to comparison with experiment, we carried the calculations until 0.25 a.u. to study mathematical aspects. Indeed, some interesting phenomena occur above the highest field of 0.12 a.u. considered until now by Alexander.[22] First, there is the semiclassical concept of a "critical field" which, by some authors (cf. e.g., Refs. 24 and 27), has been defined as the field at which the top of the potential barrier just touches the resonance level. As seen from Figs. 9 and 10, the trajectories of the complex poles do not exhibit any particular misbehavior in these regions which are characterized by the disappearance of the classical turning points. The transition from "tunneling through a potential barrier" to "feeling the barrier below" is a perfectly continuous one from the wave-mechanical point of view.

Another observation we were able to make concerns the problem of proper definition of the resonance energy. As already mentioned, our approach is to let the position of the complex pole determine both the resonance energy and the lifetime. The question arises now whether the result obtained via the phase-shift method is completely equivalent.

Alexanders's results up to 0.11 a.u. seem to confirm this hypothesis. However, led by our observation (cf. Figs. 4–6) that the zero of $\mathrm{Re}[m(E)]$ coincides almost exactly with the maximum of $\mathrm{Im}[m(E)]$ for small fields, whereas significant discrepancies first appear about 0.12 a.u., we were interested in comparisons even above this value of the field strength.

In note 23, Ref. 22, Alexander declares that by his method it was not possible to detect any resonance behavior above 0.12 a.u. It is true that the WKB connection formula he used depends on the existence of classical turning points, but according to our results they exist at least up to 0.15 a.u. Therefore we checked his results, replacing his numerical "boundary-condition method" by our Runge-Kutta integration. Agreement could be found up to 0.11 a.u., but from 0.12–0.15 a.u. (we could hence not confirm Alexander's observation) the phase-shift results did no longer coincide with the ones listed in Table I. Instead the "phase-shift resonances" seem to be close to the positions of the zeros of $\mathrm{Re}[m(E)]$.

Another phenomenon which does not occur in a very pronounced way as long as the pole is close to the real axis (or, in the discrete case, as long as ϵ is chosen to be small) is the asymmetry of the shapes of both the m function and the phase shift

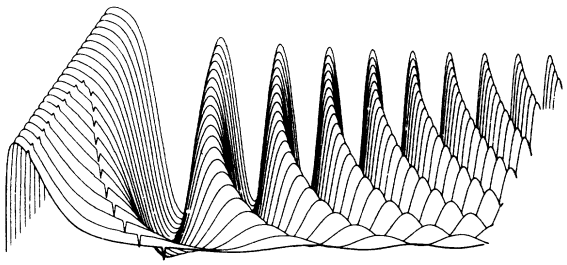

FIG. 14. Perspective view of $\psi(\eta;F)$ according to Eq. (51b). The curve in the foreground shows the wave function for $F = 0.05$ a.u., $0.0 \leq \eta \leq 56.0$ a.u., $E = E_{\mathrm{res}}$, and $Z_2 = Z_{2,\mathrm{s.c.}}$. The subsequent curves arise from increases in F of 0.01 a.u., respectively, up to 0.25 a.u. Again the spikes mark classical turning points.

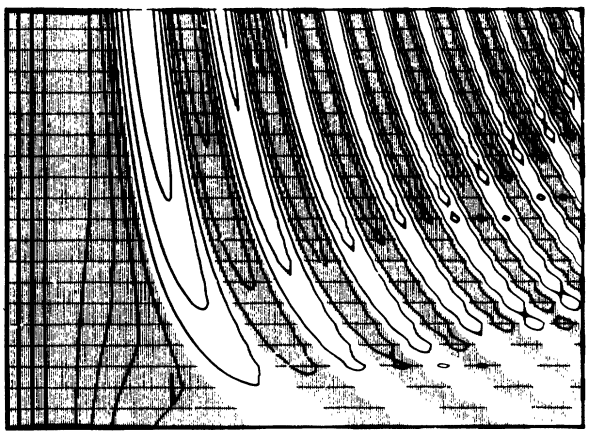

FIG. 15. Contours of $\psi(\eta;F)$, displaying the same data as plotted in Fig. 14. Abscissa is η of $0.0 \leq \eta \leq 56.0$ a.u.; ordinate is field for $0.05 \leq F \leq 0.025$ a.u. Borders between shaded and unshaded regions mark nodes of the wave functions. Note the increase of amplitudes and the number of nodes in the oscillating region of ψ for increasing F.

with respect to variation of the energy about the resonance. In the region of extremely high fields it is hence necessary to go beyond both the simple fitting of Im(m) to a Lorentzian and the Breit-Wigner parametrization of the phase shift.

ACKNOWLEDGMENTS

Michael Hehenberger has presented parts of the results at the International Workshop and Symposium at Sanibel Island, 1973, and at the Beito Symposium, 1973, and wants to thank the organizers, the University of Uppsala, and the University of Florida, for their support. We thank Professor P.-O. Löwdin for much interest and particularly for his help in connection with the asymptotic solutions. Fil.kand. Piotr Froelich assisted in the development of the pole-finding program. We are further grateful to Docent J.-L. Calais, Docent O. Goscinski and Fil.mag. R. Ahlberg for critical reading of the first draft of the manuscript.

---

*Supported by the Swedish Natural Sciences Research Council.

†Permanent address: Escuela Superior de Fisica y Matematicas, Instituto Politecnico Nacional, Mexico City, Mexico.

‡Consultant, Instituto Nacional de Energia Nuclear, Mexico City, Mexico.

[1]Hermann Weyl, Math. Ann. 68, 220 (1910).
[2]E. C. Titchmarsh, Proc. R. Soc. A 207, 321 (1951).
[3]E. C. Titchmarsh, Proc. R. Soc. A 210, 30 (1952).
[4]E. C. Titchmarsh, J. Analyse Math. 4, 187 (1954–56).
[5]E. C. Titchmarsh, *Eigenfunction Expansions Associated with Second-Order Differential Equations* (Oxford U. P., London, 1946), Vols. 1 and 2.
[6]E. A. Coddington and N. Levinson, *Theory of Ordinary Differential Equations* (McGraw-Hill, New York, 1955).
[7]Z. Kopal, *Numerical Analysis* (Wiley, New York, 1955).
[8]D. Sarofyan, J. Math. Anal. Appl. 40, 436 (1972).
[9]J. Stark, Berl. Berichte 20 (1913).
[10]H. A. Kramers, Z. Phys. 3, 199 (1920).
[11]P. S. Epstein, Ann. Phys.(Leipz.)(4) 50, 489 (1916).
[12]K. Schwarzschild, Sitzungsber. Dtsch. Akad. Wiss. Berl. Kl. Math. Phys. Tech. 548 (1916).
[13]E. Schrödinger, Ann. Phys.(Leipz.)(4) 80, 437 (1926).
[14]P. S. Epstein, Phys. Rev. 28, 695 (1926).
[15]I. Waller, Z. Phys. 38, 635 (1926).
[16]H. Rausch v. Traubenberg *et al.*, Naturwissenschaften 18, 417 (1930).
[17]C. Lanczos, Naturwissenschaften 18, 329 (1930); Z. Phys. 62, 518 (1930); 65, 431 (1930); 68, 204 (1931).
[18]G. Gamow, Z. Phys. 51, 204 (1928).
[19]R. W. Gurney and E. U. Condon, Phys. Rev. 33, 127 (1929).
[20]M. H. Rice and R. H. Good, Jr., J. Opt. Soc. Am. 52, 239 (1962).
[21]S. C. Miller, Jr. and R. H. Good, Jr., Phys. Rev. 91, 174 (1953).
[22]M. H. Alexander, Phys. Rev. 178, 34 (1969).
[23]C. M. Rosenthal and E. B. Wilson, Jr., Phys. Rev. Lett. 19, 143 (1967).
[24]J. O. Hirschfelder and L. A. Curtiss, J. Chem. Phys. 55, 1395 (1971).
[25]J. D. Bekenstein and J. B. Krieger, Phys. Rev. 188, 130 (1969).
[26]L. B. Redei, Phys. Lett. 1, 191 (1962).
[27]L. B. Mendelsohn, Phys. Rev. 176, 90 (1968).
[28]H. A. Bethe and E. E. Salpeter, *Quantum Mechanics of One- and Two-Electron Atoms* (Springer, Berlin, 1957).
[29]P. Moon and D. E. Spencer, *Field Theory Handbook* (Springer, Berlin, 1961), p. 34.
[30]H. Jeffreys, Philos. Mag. (7) 33, 451 (1942).
[31]J. C. P. Miller, *The Airy Integral* (British Assoc. for the Advancement of Science, Cambridge, 1946).
[32]G. N. Watson, *Treatise on the Theory of Bessel Functions* (Cambridge U. P., Cambridge, England, 1922).
[33]R. G. Gordon, J. Chem. Phys. 51, 14 (1969).